nature neuroscience

Selective synaptic remodeling of amygdalocortical connections associated with fear memory

Yang Yang[1,5], Dan-qian Liu[1,2,5], Wei Huang[1,4], Juan Deng[1,2], Yangang Sun[1], Yi Zuo[3] & Mu-ming Poo[1]

Neural circuits underlying auditory fear conditioning have been extensively studied. Here we identified a previously unexplored pathway from the lateral amygdala (LA) to the auditory cortex (ACx) and found that selective silencing of this pathway using chemo- and optogenetic approaches impaired fear memory retrieval. Dual-color *in vivo* two-photon imaging of mouse ACx showed pathway-specific increases in the formation of LA axon boutons, dendritic spines of ACx layer 5 pyramidal cells, and putative LA–ACx synaptic pairs after auditory fear conditioning. Furthermore, joint imaging of pre- and postsynaptic structures showed that essentially all new synaptic contacts were made by adding new partners to existing synaptic elements. Together, these findings identify an amygdalocortical projection that is important to fear memory expression and is selectively modified by associative fear learning, and unravel a distinct architectural rule for synapse formation in the adult brain.

Associative learning enables an animal to adapt to and survive in a complex environment. In classical auditory fear conditioning, animals learn to associate a neutral stimulus (a sound) with a foot shock, and they exhibit fear responses to the sound presentation. The amygdala is critical for the formation of auditory fear memory[1]. Previous studies have also shown that the ACx is required for auditory fear learning[2–4] and that fear conditioning can induce rapid and long-term changes in neuronal responses and spine dynamics in ACx[5,6]. However, which synapses in ACx undergo modification remains unclear.

Long-term *in vivo* two-photon imaging has been used to monitor structural remodeling of synaptic connectivity, as shown by changes in presynaptic boutons or postsynaptic spines that represent the formation or elimination of synapses[7,8]. Previous studies have shown that sensory experience and learning can induce changes in the turnover of presynaptic axon boutons[9] and postsynaptic dendritic spines[6,10–15]. To further explore synaptic dynamics in specific pathways, concurrent imaging of pre- and postsynaptic structures in identified connections is required. This approach, although successfully applied in studying synaptic dynamics in hippocampal slices[16], has not been used for *in vivo* imaging of the neocortex.

In this study, combining tracing methods with electron microscopy, we identified a projection to ACx that originates from LA, the major input region of the amygdala. Chemo- and optogenetic silencing of LA axons in ACx during fear recall testing greatly reduced animals' fear responses, suggesting that the LA–ACx pathway is important to the expression of fear memory. By jointly imaging labeled axons originating from brain regions projecting to ACx and apical dendrites of pyramidal neurons in ACx, we were able to monitor the dynamics of putative synaptic pairs in specific pathways *in vivo*. We observed a selective increase in bouton and spine formation at LA–ACx connections after fear conditioning, resulting in a gradual increase of LA–ACx synapses. By contrast, no fear-memory-related synaptic rewiring was observed in connections from the medial geniculate body (MG) or anterior cingulate cortex (ACC) to ACx. Furthermore, concurrent imaging of pre- and postsynaptic structures showed that nearly all newly formed synaptic contacts were made by adding new boutons to existing spines or new spines to existing boutons. These findings reveal an amygdalocortical projection involved in fear memory expression and suggest an architectural rule for synapse formation in the adult brain.

RESULTS

Fear learning with complex sound requires auditory cortex

Previous work has suggested that ACx is not required for auditory fear learning when pure tones are used as conditioned stimulus (CS)[17]. We thus used a train of short beeps, which coterminated with a foot shock, for fear conditioning (**Fig. 1a**). Conditioned mice received five repeats of the CS paired with a foot shock, whereas control mice received five repeats of explicitly unpaired CS and foot shock. Animals were tested with CS 1 d after conditioning. Conditioned mice showed significantly higher freezing responses than control mice (**Fig. 1a** and **Supplementary Fig. 1a**).

We found that bilateral infusion of the $GABA_A$ receptor agonist muscimol or NMDA receptor antagonist (*2R*)-amino-5-phosphonopentanoate (APV)[18] in ACx before fear conditioning largely prevented the mice from developing postconditioning freezing responses, suggesting that the activity and NMDA receptor-dependent plasticity in ACx were necessary for auditory fear conditioning (**Fig. 1b** and **Supplementary Figs. 1b**,**c** and **2**). Infusion of both drugs immediately after conditioning also impaired fear responses, indicating that activity and plasticity in ACx in the postconditioning period

[1]Institute of Neuroscience, State Key Laboratory of Neuroscience, CAS Center for Excellence in Brain Science and Intelligence Technology, Shanghai Institutes for Biological Sciences, Chinese Academy of Sciences, Shanghai, China. [2]Institute of Neuroscience, Graduate School, University of Chinese Academy of Sciences, Beijing, China. [3]Department of Molecular, Cell and Developmental Biology, University of California Santa Cruz, Santa Cruz, California, USA. [4]Present address: Eli and Edythe Broad Center of Regeneration Medicine and Stem Cell Research, University of California San Francisco, San Francisco, California, USA. [5]These authors contributed equally to this work. Correspondence should be addressed to Y.Y. (yangyang@ion.ac.cn).

Received 6 May; accepted 29 June; published online 5 September 2016; doi:10.1038/nn.4370

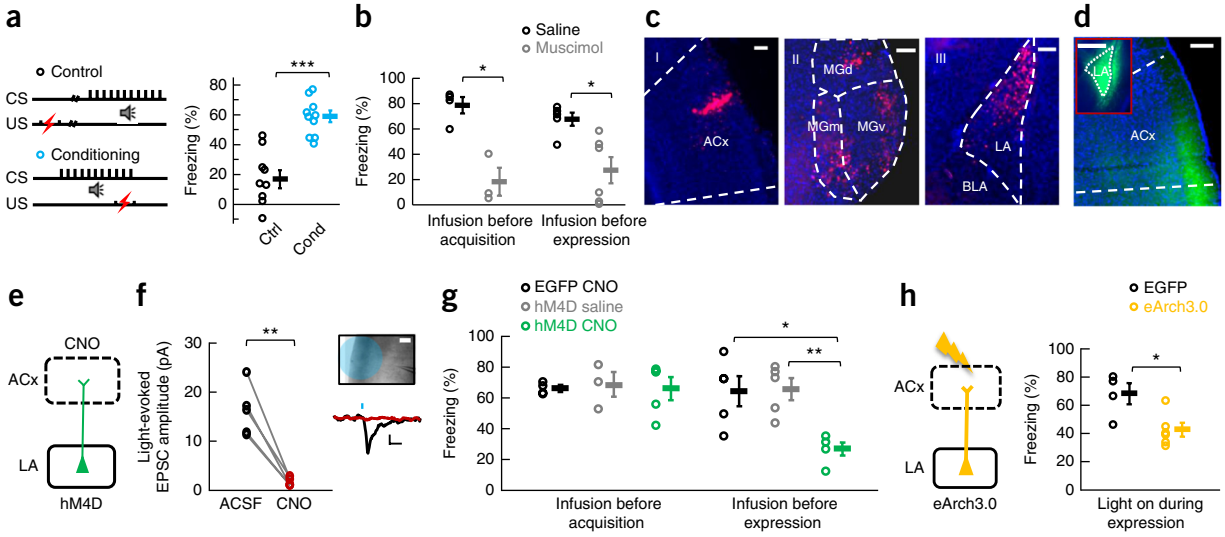

Figure 1 Projections from LA to ACx were important for fear memory expression. (**a**) Left: fear conditioning protocols. Conditioned mice received five repeats of paired sound and foot shock. Control mice received five repeats of explicitly unpaired sound and foot shock. Right: CS sound-triggered freezing responses of control (Ctrl, $n = 9$) and conditioned (Cond, $n = 10$) mice in a new context. Student's t-test, $t(17) = 7$, $P = 3 \times 10^{-6}$. (**b**) Freezing responses in recall test for mice bilaterally infused with muscimol 30 min before fear conditioning (saline, $n = 4$; muscimol, $n = 3$; $t(5) = 4$, $P = 0.01$) or recall test (saline, $n = 5$; muscimol, $n = 6$; $t(9) = 3$, $P = 0.01$). Student's t-test. (**c**) Retrograde labeling of neurons projecting to ACx. Left, Retrobead injection site in ACx; right and center, retrogradely labeled neurons in MG and LA. MGd, dorsal MG; MGv, ventral; MGm, medial. Scale bars, 100 µm. (**d**) Image showing anterogradely labeled LA axons in ACx. Scale bar, 500 µm. Red box, virus injection site in LA. Scale bar, 200 µm. (**e**) Selective silencing of the LA–ACx pathway using DRREAD system. AAV-hM4D (or AAV-EGFP, as a control) was injected into LA, and CNO (or saline, as a control) was infused locally into ACx. (**f**) Light-evoked excitatory synaptic currents (EPSCs) recorded from postsynaptic ACx neurons before (black) and after (red) CNO perfusion ($n = 5$ neurons). Paired t-test, $t(4) = 7$, $P = 0.002$. Upper inset shows a recorded neuron in L5. Blue circle shows light illumination area. Blue light is limited to the superficial layers of ACx. Scale bar, 100 µm. Lower inset shows an example of a light-evoked EPSC trace. Scale bar, 10 pA, 25 ms. (**g**) Freezing responses of mice expressing hM4D (or EGFP) in LA infused with CNO (or saline) in ACx before fear acquisition (EGFP CNO, $n = 4$; hM4D saline, $n = 3$; hM4D CNO, $n = 5$; EGFP CNO vs. hM4D CNO, $t(7) = 0.02$, $P = 1$; hM4D saline vs. hM4D CNO, $t(6) = 0.2$, $P = 0.8$) or expression (EGFP CNO, $n = 5$; hM4D saline, $n = 5$; hM4D CNO, $n = 4$; EGFP CNO vs. hM4D CNO, $t(7) = 3$, $P = 0.02$; hM4D saline vs. hM4D CNO, $t(7) = 4$, $P = 0.004$. Student's t-test). (**h**) Left: diagram showing selective silencing of LA–ACx pathway using optogenetics. AAV-eArch3.0 or AAV-EGFP was injected into LA and superficial layers of ACx were illuminated by yellow light. Right: freezing responses of mice expressing eArch3.0 ($n = 6$) or EGFP ($n = 4$) in LA with light on in ACx during expression. Student's t-test, $t(8) = 3$, $P = 0.02$. Error bars in **a**,**b**,**g**,**h**, s.e.m.

were also required for postconditioning fear memory consolidation (**Supplementary Fig. 1d**). Furthermore, inactivation of ACx by muscimol injection immediately before the recall test also reduced freezing responses (**Fig. 1b**). Thus, ACx is required for both acquisition and expression of auditory fear memory.

LA–ACx pathway plays a key role in fear memory expression

Layer (L) 1 of sensory cortices receives long-range inputs from higher order brain regions that are involved in different behaviors[19,20]. To examine the origins of the long-range projections to ACx, we injected retrograde fluorescent microspheres (Retrobeads) into the superficial layers of ACx (**Fig. 1c**). We observed densely labeled neurons in the medial geniculate body (**Fig. 1c**), including the medial division that showed fear conditioning-induced changes[21]. Unexpectedly, we also found retrograde labeling in LA (**Fig. 1c**), which was previously considered to be an input region of the amygdala[22]. We injected an adeno-associated virus (AAV) containing an EGFP expression construct into LA and found LA axons terminating in ACx, thus confirming that LA sent direct projections to ACx (**Fig. 1d**).

To explore whether this pathway is involved in fear learning and memory, we used the designer receptors exclusively activated by designer drugs (DREADD) system—G_i-protein-coupled receptor hM4D and its ligand clozapine-*N*-oxide (CNO)—to selectively silence the LA–ACx pathway during fear acquisition or expression[23,24] (**Fig. 1e**). We first validated that local CNO application in ACx could inhibit synaptic transmission of hM4D-expressing LA axons using slice recording[25]. We co-injected AAV-ChR2 and AAV-hM4D into LA (**Supplementary Fig. 3**) and performed whole-cell recordings on ACx L5 neurons in coronal brain slices containing ACx neurons and axons from LA. We recorded light-evoked excitatory postsynaptic currents (EPSCs) with blue light on the superficial layers of ACx, where LA axons terminate. We found that addition of CNO to the recording solution completely abolished the light-evoked responses (5 cells from 3 animals, $P = 0.003$, paired t-test, **Fig. 1f**). To examine how selective silencing of LA–ACx pathway affects behavior, we inhibited the synaptic transmission of the LA–ACx pathway by expressing hM4D in LA and locally infusing CNO into ACx, during either fear conditioning or the fear recall test (**Fig. 1e** and **Supplementary Fig. 4a**). Because of the low success rate in targeting LA for virus injection, we inhibited the LA–ACx pathway unilaterally and infused muscimol to silence the contralateral ACx. In control experiments, during fear conditioning or recall, we silenced the right side of ACx with muscimol and either infused CNO into left ACx of mice injected with AAV-EGFP in left LA or infused saline into left ACx of mice injected with AAV-hM4D in left LA. In all cases, mice exhibited strong freezing responses (**Fig. 1g**). In chemogenetic inactivation experiments, we also silenced the right side of ACx with muscimol but infused CNO into left ACx of mice injected with AAV-hM4D in left LA. We found that the chemogenetic inactivation of LA–ACx pathway during fear recall testing but not fear learning significantly impaired animals' fear responses (**Fig. 1g** and **Supplementary Fig. 4b**), indicating that this pathway is involved in the expression of fear memory.

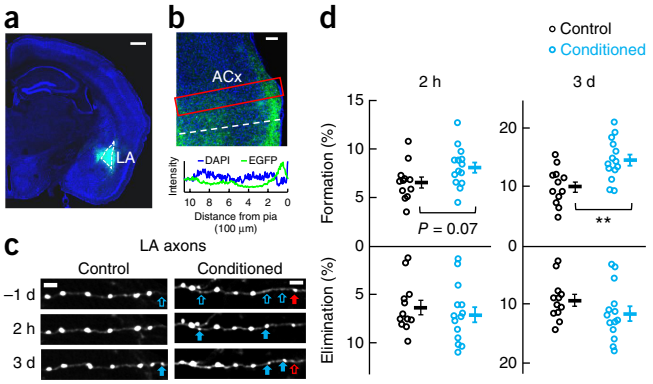

Figure 2 Fear conditioning induces increase in bouton formation in LA axons that terminate in L1 of ACx. (**a**) AAV-EGFP injection site in LA. Green, GFP; blue, DAPI. Scale bar, 500 µm. (**b**) Top: EGFP-expressing LA axons in ACx. Scale bar, 100 µm. Bottom: intensity profile of DAPI and EGFP signals in ACx along the red rectangle (top). EGFP signals are detected mostly in L1. (**c**) Example images obtained by repeated imaging of the same LA axons in L1 of ACx in control and conditioned animals at 1 d before (–1 d) and 2 h or 3 d after conditioning. Cyan arrows, newly formed boutons, as compared to –1 d; red arrows, eliminated boutons. Open arrows: position of to-be-formed or eliminated boutons; filled arrows: newly formed or to-be-eliminated boutons. Scale bar, 4 µm. (**d**) Percentages of newly formed and eliminated boutons in control and conditioned mice for LA axons in L1 of ACx at 2 h and 3 d, relative to the bouton number at –1 d. Circles, results from individual mice (conditioned, $n = 14$; control, $n = 12$). Mann-Whitney U test, 2 h, formation, $U = 126$, $P = 0.07$; 2 h, elimination, $U = 147$, $P = 0.5$; 3 d, formation, $U = 105$, $P = 0.003$; 3 d, elimination, $U = 129$, $P = 0.1$. For each mouse, over 200 boutons were included in the analysis. Error bars, s.e.m.

Similarly, we performed pathway-specific optogenetic experiments by photoinhibiting archaerhodopsin (eArch3.0)-expressing LA axons in ACx during fear recall tests (**Fig. 1h** and **Supplementary Fig. 4c**). As in the experiments using DREADDs, the LA–ACx pathway was inhibited unilaterally and we infused muscimol into the contralateral ACx. We found that optogenetic inhibition of LA–ACx pathway could also impair fear memory recall (**Fig. 1h**). Together, these results showed that LA projects directly to ACx, and this projection is important for the expression of fear memory.

Bouton formation in LA axons increases after conditioning

To examine the structural plasticity of LA projections in ACx associated with fear memory, we injected AAV-SYN-EGFP into LA and imaged the labeled LA axons in L1 of ACx (**Fig. 2a**,**b**). Boutons on these LA axons were mostly *en passant* boutons, in contrast to *terminaux* boutons along the axons of L6 pyramidal cells[26]. To search for conditioning-induced presynaptic structural changes, we imaged the same set of boutons (**Fig. 2c**; see **Supplementary Fig. 5** for the criterion; see also ref. 26) 1 d before as well as 2 h and 3 d after conditioning. We calculated percentages of bouton formation and elimination by comparing the images obtained 2 h and 3 d after conditioning with those obtained 1 d before conditioning. Consistent with previous findings[9,26], only small percentages of boutons underwent turnover with time in control adult mice (**Fig. 2d**). Compared with control mice that received unpaired CS and foot shock, the percentages of newly formed boutons in conditioned mice were slightly higher at 2 h (8.0 ± 0.6% vs. 6.5 ± 0.6%, $P = 0.07$, **Fig. 2d**) and became significantly higher at 3 d (14.4 ± 0.9% vs. 9.9 ± 0.9%; $P = 0.003$, **Fig. 2d**). By contrast, no difference was found for the percentages of eliminated boutons between conditioned and control groups ($P = 0.1$, **Fig. 2d**). Therefore, remodeling of LA axons in ACx is associated with fear learning.

No changes in bouton dynamics in MG and ACC axons

L1 of ACx also receives inputs from the medial division of MG (**Fig. 1c**; see also ref. 27), which is known to exhibit auditory fear conditioning-induced plasticity[21]. To explore whether MG projections in ACx undergo conditioning-induced structural modification, we injected AAV containing human synapsin promoter–driven EGFP (AAV-SYN-EGFP) into mouse MG (**Fig. 3a**,**b**) and imaged the MG axons in L1 of ACx before and after fear conditioning (**Fig. 3c**). We found no difference in the rate of bouton formation or elimination between conditioned and control mice (2 h, formation, $P = 1$; elimination, $P = 0.3$; 3d, formation, $P = 0.7$; elimination, $P = 0.4$; **Fig. 3d**). In addition to LA and MG, ACx receives long-range feedback projections from ACC (**Supplementary Fig. 6**; see also ref. 28), which is also known to be involved in fear conditioning[29]. Similar imaging experiments of ACC axons in L1 of ACx showed no conditioning-induced change in bouton formation or elimination (**Fig. 3e–h**). Taken together, these results indicate that fear conditioning induces a behavior-correlated increase of axon boutons only in LA axon inputs and that it does so by increasing the rate of bouton formation without affecting that of bouton elimination.

LA axon boutons form synapses with L5 neurons in L1 of ACx

Long-range connections could serve as a substrate for long-term memory storage, via behavior-induced plasticity[30,31]. Having found that formation of LA boutons in ACx is selectively elevated after fear conditioning, we then set out to explore the postsynaptic partners of these boutons. Previous studies have shown that long-range projections from subcortical areas innervate distal apical dendrites of L5 cortical pyramidal neurons[32,33]. To examine whether LA axon boutons made direct synaptic contact with L5 neurons in L1 of ACx, we performed immunogold electron microscopy. We first injected AAV that expresses Cre recombinase into LA of YFP-H mice[34], in which a small population of L5 cortical neurons expresses YFP, and immunostained Cre and YFP with different gold particles. We found that Cre-labeled LA boutons formed asymmetric synapses with YFP-labeled spines in L1 of ACx (**Fig. 4a**), confirming that the L1 apical dendrites originating from L5 neurons in ACx receive direct synaptic inputs from LA neurons.

Spine formation in ACx L5 cells increases after conditioning

We next investigated whether there are conditioning-induced changes in L1 spine of L5 neurons in ACx by measuring spine turnover rate in apical dendrites with *in vivo* two-photon imaging. Using YFP-H transgenic mice, we found that the percentages of newly formed spines on apical dendrites of L5 neurons were significantly higher in fear-conditioned mice than those in control mice at 3 d after conditioning (10.0 ± 0.7% vs. 6.7 ± 0.7%; $P = 0.002$; **Fig. 4b**,**c**), but not at 2 h (5.0 ± 0.6% vs. 4.8 ± 0.5%; $P = 1.0$; **Fig. 4b**,**c**). Further analysis showed a tendency for correlation between spine formation rate and freezing responses of fear conditioned animals (**Supplementary Fig. 7**). No change in spine elimination was observed (2 h, $P = 0.2$; 3 d, $P = 0.7$; **Fig. 4b**,**c**). These results were consistent with the previous finding that spines formed in ACx during auditory fear conditioning can persist for a long time[6]. Our failure to see a transient increase at 2 h, as was reported in ref. 6, could be due to the difference in the imaged population of labeled neurons in different transgenic lines[34].

To examine whether the increase in spine formation after fear conditioning is specific to apical dendrites of L5 neurons in ACx, we

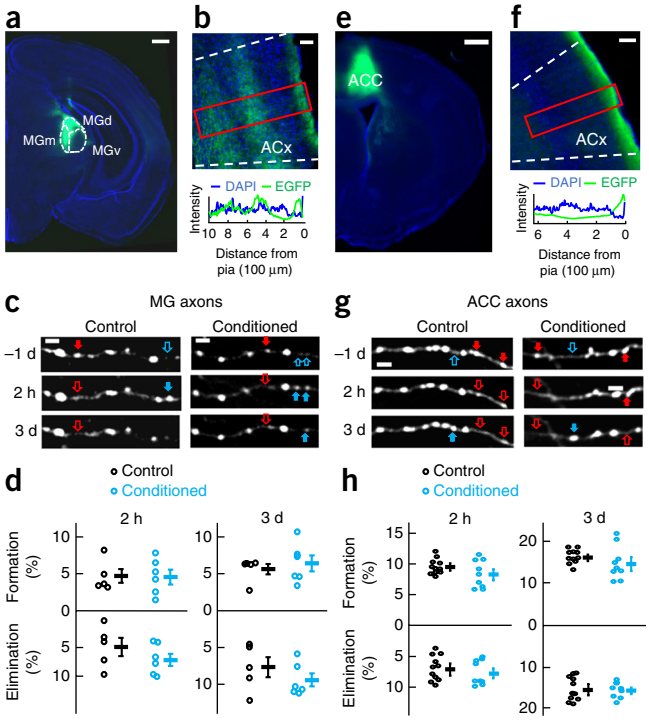

Figure 3 No changes in the bouton dynamics of MG or ACC axons in L1 of ACx. (**a**) Image showing AAV-SYN-EGFP injection site in MG, including medial and dorsal (MGm and MGd, respectively). Green, GFP; blue, DAPI. Scale bar, 500 μm. (**b**) Top: EGFP-expressing MG axons in ACx. Scale bar, 100 μm. Bottom: intensity profile of DAPI and EGFP signals in ACx along the red rectangle. EGFP signals are detected in L1, L4 and L6. (**c**) Examples of repeated imaging of the same MG axons in L1 of ACx in control and conditioned animals at –1 d, 2 h and 3 d. Cyan arrows, newly formed boutons, as compared to –1 d; red arrows, eliminated boutons. Open arrows: position of to-be-formed or eliminated boutons; filled arrows: newly formed or to-be-eliminated boutons. Scale bars, 4 μm. (**d**) Percentages of newly formed and eliminated MG boutons in control and conditioned mice at 2 h and 3 d, as compared to –1 d. (conditioned, $n = 5$; control, $n = 6$). Mann-Whitney U test,2 h, formation, $U = 30$, $P = 1$; 2 h, elimination, $U = 23$, $P = 0.3$; 3 d, formation, $U = 27$, $P = 0.7$; 3 d, elimination, $U = 25$, $P = 0.4$. (**e**–**h**) As in **a**–**d**, respectively, except that the labeled neurons were in ACC and the imaged axon boutons in L1 of ACx were ACC axons (conditioned, $n = 9$; control, $n = 11$). Mann-Whitney U test, 2 h, formation, $U = 78$, $P = 0.2$; 2 h, elimination, $U = 106$, $P = 0.4$; 3 d, formation, $U = 74$, $P = 0.1$; 3 d, elimination, $U = 97$, $P = 0.9$. Error bars, s.e.m. Scale bar: 500 μm in **e**, 100 μm in **f**, 4 μm in **g**.

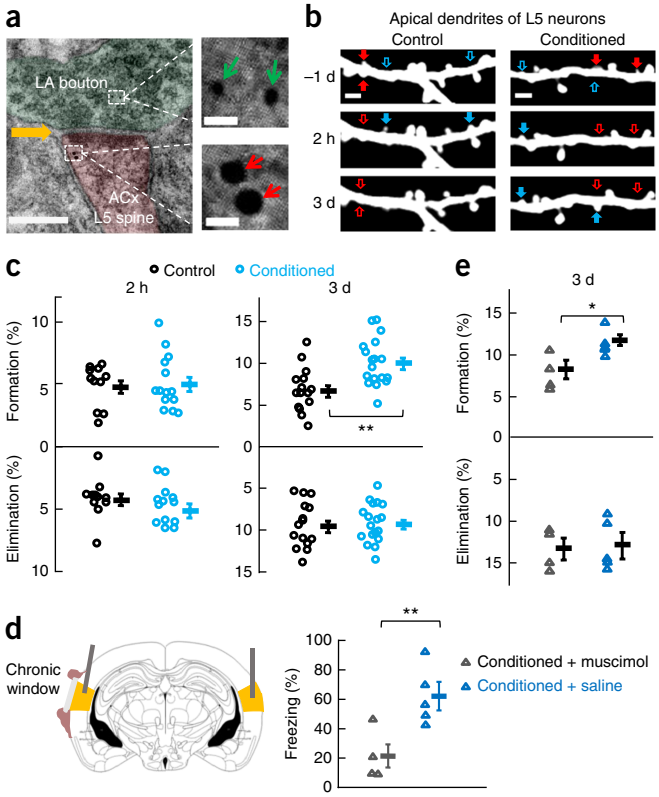

Figure 4 Significant increases in spine formation 3 d after conditioning in the apical dendrites of L5 neurons in ACx. (**a**) Electron micrographs of dual immunogold-labeling of ACx slices, showing that LA axons (green) formed an asymmetric synapse (yellow arrow) with ACx L5 neurons (red) in L1. Red arrows (bottom), 15-nm Nanogold particles that immunolabeled YFP expressed in ACx L5 neurons; green arrows (top), 5-nm Nanogold particles that immunolabeled Cre-expressing LA neurons. Scale bars: 200 nm (left); 20 nm (right). (**b**) Example images obtained by repeated imaging of the same apical dendrites of ACx L5 neurons in control and conditioned mice. Cyan and red arrows, newly formed and eliminated spines, respectively, as compared to –1 d. Open arrows: position of to-be-formed or eliminated spines; filled arrows: newly formed or to-be-eliminated spines. Scale bars, 2 μm. (**c**) Percentages of spine formation and elimination at apical dendrites of L5 neurons in control and conditioned mice at 2 h (conditioned, $n = 14$; control, $n = 11$; formation, $U = 142$, $P = 1$; elimination, $U = 118.5$, $P = 0.2$) and 3 d (conditioned, $n = 18$; control, $n = 15$; formation, $U = 169$, $P = 0.002$; elimination, $U = 268$, $P = 0.7$). Mann-Whitney U test. (**d**) Freezing responses of animals with chronic windows, infused bilaterally with muscimol or saline in ACx at 30 min before fear conditioning (muscimol, $n = 4$; saline, $n = 5$). Students' t-test, $t(7) = 4$, $P = 0.01$. (**e**) Percentages of spine formation and elimination in the same group of conditioned mice as in **d** at 3 d (muscimol, $n = 4$; saline, $n = 5$). $U = 11$, $P = 0.03$ for formation, $U = 23$, $P = 0.6$ for elimination. Mann-Whitney U test. For each mouse, over 200 spines were included for analysis. Error bars, s.e.m.

labeled L2/3 neurons with fluorescent protein tdTomato via *in utero* electroporation (**Supplementary Fig. 8a**,**b**) and performed similar imaging experiments. Neither spine formation nor elimination was changed in the apical dendrites of L2/3 neurons (**Supplementary Fig. 8c**,**d**). Thus, fear conditioning-induced changes in spine formation of the apical dendrites in L1 were not part of a general change in spine dynamics in ACx, but rather specific to L5 pyramidal neurons.

Blocking fear memory prevents increase in spine formation

To determine whether the changes in spine dynamics were linked to fear learning, we bilaterally infused muscimol into ACx of YFPH mice, which were implanted with cranial chronic windows for two-photon imaging (**Fig. 4d**). We found that, as muscimol infusion impaired fear memory, it also prevented any fear-conditioning-induced changes in the dynamics of spines on apical dendrites of L5 neurons ($P = 0.03$, **Fig. 4d**,**e**). This result further supports the notion that synaptic changes in ACx are associated with fear memory.

Pathway-specific changes in bouton and spine dynamics

Spines on the same dendrite could respond differently during a certain behavioral task[35], possibly as a result of different inputs[36]. It is thus of interest to determine whether spines on the same dendrite can exhibit different plasticity and, if so, whether different origins of the inputs can account for this difference. Similarly, boutons along the same axon show highly correlated and yet variable activity patterns[37]. Postsynaptic signals also could affect the presynaptic functional and

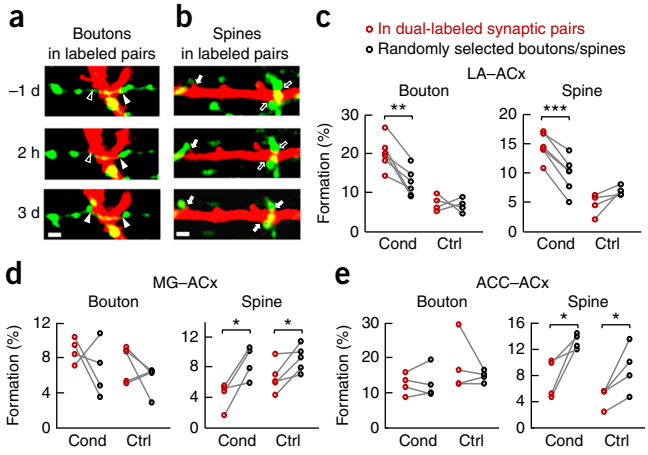

Figure 5 Fear conditioning-induced increases in bouton and spine formation were specific to LA–ACx connections. (**a**,**b**) Images obtained using dual-color *in vivo* two-photon imaging of LA axons (green) and ACx L5 neurons (red) at –1 d, 2 h and 3 d. (**a**) Triangles indicate LA boutons with labeled postsynaptic partners (L1 spines of ACx L5 neurons). Open triangles: position of to-be-formed or eliminated boutons; filled triangles: newly formed or stable boutons. (**b**) Arrows indicate spines on apical dendrites of L5 neurons with labeled presynaptic partners (LA boutons). Open arrows: position of to-be-formed spines; filled arrows: newly formed or stable spines. Scale bars: 2 µm. (**c**) Percentages of newly formed boutons or spines in labeled LA–ACx synaptic pairs (red circles), as compared to those in randomly selected boutons or spines in the same animal (black circles), in conditioned (Cond, $n = 6$) and control (Ctrl, $n = 4$) mice at 3 d after conditioning. Bouton, $t(5) = 5$, $P = 0.004$ in Cond, $t(3) = 0.3$, $P = 0.8$ in Ctrl; spine, $t(5) = 8$, $P = 0.0004$ in Cond, $t(3) = 2$, $P = 0.1$ in Ctrl. Paired *t*-test. (**d**,**e**) As in **c**, except that labeled synaptic pairs were in MG–ACx (Cond, $n = 4$; Ctrl, $n = 5$; bouton, $t(3) = 1$, $P = 0.4$ in Cond, $t(4) = -0.2$, $P = 0.8$ in Ctrl; spine, $t(3) = 4$, $P = 0.04$ in Cond, $t(4) = 3$, $P = 0.04$ in Ctrl; paired *t*-test) or ACC–ACx connections (Cond, $n = 4$; Ctrl, $n = 4$; bouton, $t(3) = 0.3$, $P = 0.8$ in Cond, $t(3) = 0.9$, $P = 0.4$ in Ctrl; spine, $t(3) = 3$, $P = 0.04$ in Cond, $t(3) = 3$, $P = 0.049$ in Ctrl; paired *t*-test).

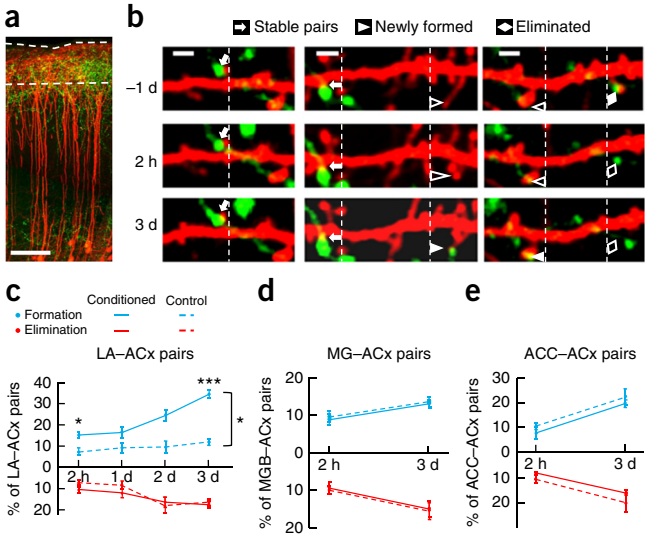

Figure 6 Conditioning-induced increase in the formation of putative synapses in LA–ACx connections. (**a**) Image of a fixed slice showing colocalization of LA axons (GFP, green) and apical dendrites of L5 neurons (YFP, red) in superficial layers of ACx. Dashed lines delimit the most superficial 100 µm from pial surface. Scale bar, 100 µm. (**b**) Images obtained using dual-color *in vivo* two-photon imaging of LA axons (green) and ACx L5 neurons (red) at –1 d, 2 h and 3 d. Arrows, triangles and diamonds point to stable, newly formed and eliminated putative synaptic pairs, respectively. Open symbols: position of to-be-formed or eliminated synapses; filled symbols: stable, newly formed or to-be-eliminated synapses. Scale bars, 2 µm. (**c**) Percentages of newly formed and eliminated LA–ACx synaptic pairs in control ($n = 4$) and conditioned mice ($n = 6$) at 2 h, 1 d, 2 d and 3 d, as compared to –1 d. Mann-Whitney *U*-test, 2 h, formation, $U = 11$, $P = 0.02$; 2 h, elimination, $U = 15$, $P = 0.2$; 3 d, formation, $U = 10$, $P = 0.001$; 3 d, elimination, $U = 20$, $P = 0.8$. Kolmogorov-Smirnov test was used for group comparison of all time points between control and conditioned mice. $P = 0.01$ for formation, $P = 0.5$ for elimination. (**d**,**e**) Percentages of newly formed and eliminated MG–ACx pairs (conditioned, $n = 4$; control, $n = 5$; 2 h, formation, $U = 18$, $P = 0.7$; 2 h, elimination, $U = 17$, $P = 0.6$; 3 d, formation, $U = 19$, $P = 0.9$; 3 d, elimination, $U = 18$, $P = 0.7$) and ACC–ACx pairs (conditioned, $n = 4$; control, $n = 4$; 2 h, formation, $U = 22$, $P = 0.3$; 2 h, elimination, $U = 20$, $P = 0.7$; 3 d, formation, $U = 19$, $P = 0.8$; 3 d, elimination, $U = 20$, $P = 0.7$) in control and conditioned mice after conditioning. Mann-Whitney *U*-test. For each mouse, around 100 synaptic pairs were included for analysis. Error bars, s.e.m.

structural plasticity[38]. Whether boutons on the same axons exhibit differential structural plasticity due to different postsynaptic connections thus remains an open question.

To examine whether the turnover dynamics of boutons and spines in ACx were differentially modulated in a pathway-specific manner, we performed concurrent two-photon imaging on long-range projecting axons and ACx dendrites. We injected AAV- EGFP into LA, MG or ACC of YFP-H mice and simultaneously imaged presynaptic GFP and postsynaptic YFP signals in ACx. GFP and YFP signals were separated using bandpass filters (Online Methods and **Supplementary Fig. 9**). We identified putative synaptic contacts using a defined morphological criterion (Online Methods; see also ref. 16). We compared the turnover of boutons and spines that contacted labeled identified synaptic partners (**Fig. 5a**,**b**) with that of randomly selected pairs of boutons and spines in the same images. We found that formation rates of boutons and spines in LA–ACx connections were higher than those in unidentified connections at 3 d in fear-conditioned mice but not in control mice (**Fig. 5c** and **Supplementary Fig. 10a**), indicating that fear learning induced an increase in bouton and spine formation in this pathway. By contrast, the formation rates of spines in MG–ACx and ACC–ACx connections were significantly lower than those of randomly selected spines in both conditioned and control mice, suggesting that the L1 spines of L5 ACx neurons that received MG and ACC inputs were more stable (**Fig. 5d**,**e** and **Supplementary Fig. 10b**,**c**). Thus, fear-conditioning-induced increases in bouton and spine formation were specific to the LA–ACx connections, indicating a pathway-specific modulation of structural changes among LA axons and ACx dendrites by fear learning.

Rapid and gradual increase in LA–ACx synapses over days

To examine the time course of synaptic modification of LA–ACx connections after fear learning, we performed daily imaging of dual-labeled LA–ACx synapses after fear conditioning, comparing images taken at 2 h, 1 d, 2 d and 3 d to those taken at 1 d before for quantification of stable, newly formed, and eliminated synaptic pairs (**Fig. 6a**,**b**). Fear memory was tested 1 d after conditioning. We found that the percentage of newly formed LA–ACx synaptic pairs started to show a significant increase in conditioned mice (15.2 ± 1.1%) compared control mice (7.4 ± 1.8%; $P = 0.02$, **Fig. 6c**) as early as 2 h after conditioning. This rapid change was not observed in either bouton or spine dynamics when their synaptic partners were unidentified. Daily imaging over the next 3 d after conditioning showed a gradual increase in the percentage

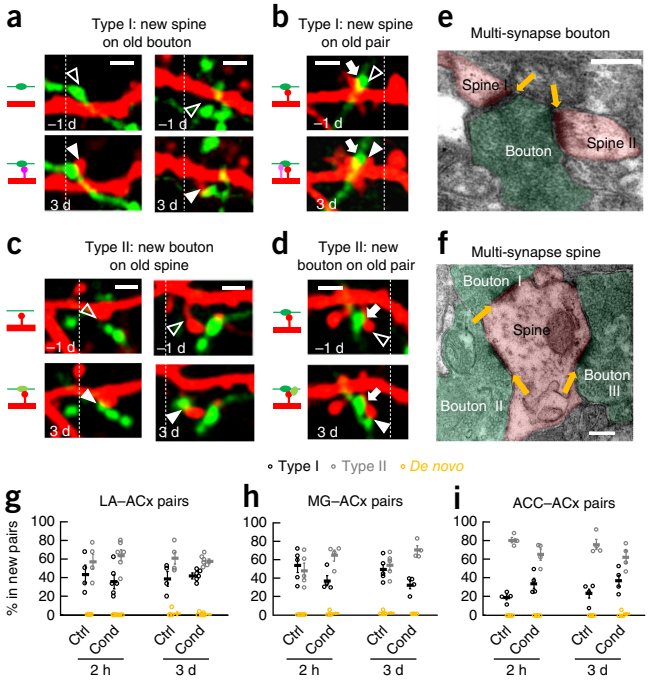

Figure 7 New synapses were made by adding new partners to existing synaptic elements. (**a**,**b**) Example images showing type I formation of synaptic pairs: new spines on existing boutons, with the postsynaptic partners unlabeled (**a**) or labeled (**b**). Scale bars: 2 µm. (**c**,**d**) Example images showing type II formation of synaptic pairs: new boutons on existing spines, with the presynaptic partners unlabeled (**c**) or labeled (**d**). Open triangles: positions of to-be-formed spines or boutons; filled triangles: newly formed spines or boutons; filled arrows, existing synapses. Scale bars: 2 µm. (**e**) Electron micrographs from L1 of ACx showing two spines (red) of ACx neurons making synaptic contacts with the same bouton (green) to form a multi-synapse bouton. Yellow arrows, asymmetric synaptic contacts. Scale bar: 200 nm. (**f**) Electron micrographs from L1 of ACx showing three boutons (green) making synaptic contacts with the same spine to form a multi-synapse spine. Scale bar: 200 nm. (**g**–**i**) The proportion of type I, type II, or *de novo* formation in newly formed LA–ACx pairs (**g**, conditioned, $n = 6$; control, $n = 4$), MG–ACx pairs (**h**, conditioned, $n = 4$; control, $n = 5$), or ACC–ACx pairs (**i**, conditioned, $n = 4$; control, $n = 4$) in control (Ctrl) and conditioned (Cond) mice at 2 h and 3 d. Error bars, s.e.m.

of newly formed synaptic pairs ($P = 0.01$, Kolmogorov-Smirnov test, **Fig. 6c**), while that of eliminated pairs maintained similar between the two groups ($P = 0.5$, **Fig. 6c**). Imaging of MG–ACx and ACC–ACx connections showed no changes in the percentages of formation or elimination of putative synaptic pairs between conditioned and control groups (MG–ACx: 2 h, formation, $P = 0.7$; elimination, $P = 0.6$; 3 d, formation, $P = 0.9$; elimination, $P = 0.7$; ACC–ACx: 2 h, formation, $P = 0.3$; elimination, $P = 0.7$; 3 d, formation, $P = 0.8$; elimination, $P = 0.7$; **Fig. 6d**,**e**). Thus, fear conditioning induced a rapid (within 2 h) elevation in the formation of new LA–ACx connections that continued over a period of days, consistent with the rapid formation and post-conditioning consolidation of fear memory[39].

'Additive' form of new synapse formation in adult brain

During data analysis of dual-color imaging studies, we discovered, unexpectedly, that new LA–ACx synaptic pairs essentially all took an 'additive' form: i.e., they were due to either the appearance of a new spine on an existing bouton ("type I"; **Fig. 7a** and **Supplementary Fig. 11a**; ~43.5%) or a new bouton on an existing spine ("type II"; **Fig. 7c** and **Supplementary Fig. 11b**; ~55%), with extremely rare occurrence (~1.5%, 4 out of 262 new pairs) of *de novo* synapse formation (**Supplementary Fig. 11c**). These existing boutons and spines are likely to have an unlabeled existing synaptic partner because there is sparse labeling of pre- and postsynaptic cells. Thus type I and type II formation may result in multi-synapse boutons and multi-synapse spines, respectively, which were indeed observed occasionally when both pre- and postsynaptic cells happened to be labeled (**Fig. 7b**,**d** and **Supplementary Fig. 11d**,**e**; 31 of 262 cases). By contrast, replacement of an existing pre- or postsynaptic element with a new one was rarely observed (2 of 262; **Supplementary Fig. 11f**). Using electron microscopy, we confirmed the existence of both multiple-synapse boutons and multiple-synapse spines in L1 of ACx of conditioned animals (**Fig. 7e**,**f**).

Similar percentages of type I and type II new synaptic pair formation were found for LA–ACx connections in control mice, as well as for MG–ACx and ACC–ACx connections in conditioned and control mice (**Fig. 7g**–**i**). Furthermore, the percentages of type II formation were in general higher than those of type I formation in both control and conditioned mice (**Fig. 7g**–**i**). Given that this mode of new synapse formation was found for all connections in ACx, addition of new partners to existing synaptic elements may represent a general architecture rule for making new synaptic connections in the adult cortex. Finally, we observed that in some cases ($n = 31$) a new bouton (or spine) added to an existing synapse was initiated by the same axon (or dendrite) that harbored the existing synapse (**Fig. 7b**,**d** and **Supplementary Fig. 11d**,**e**), thus strengthening the connections between existing neuronal partners. This result is consistent with previous findings that, after LTP induction, multiple spines from the same dendrite made contacts with the same presynaptic axon bouton[40]. Such synapse addition could also lead to spatially clustered spines that are more likely to be coactive[41], providing a potential explanation for spatial clustering of learning-induced new spine formation[12,42].

DISCUSSION

The neural circuits underlying auditory fear conditioning have been extensively characterized. Auditory information flows from the auditory thalamus and ACx to the LA, then to the basolateral amygdala and the central amygdala, which projects to the brainstem that controls fear responses[1,22]. In this study, we identified a feedback pathway from LA to ACx and showed that this pathway is important for the expression of fear memory. Specifically inhibiting this pathway during fear recall testing using the DREADD system or optogenetics significantly reduced fear responses. By contrast, we found no effect when the pathway was inhibited before fear learning. Nevertheless, we cannot exclude the possibility that the LA–ACx pathway also contributes to fear learning, because we could at best partially block LA–ACx connections using the current method, owing to limited virus expression in LA.

Synaptic connections were modified by experience, providing a substrate for learning and memory. Sensory experience, motor learning and aging were all found to induce changes in the dynamics of presynaptic axon boutons or postsynaptic dendritic spines[6,9,10,12–15]. Whereas both boutons and spines could represent synaptic connections on their own[7,8,10–14], concurrent imaging of pre- and postsynaptic structures provides more information on pathway specificity. In this study, we found that fear learning induced structural remodeling specifically at LA–ACx connections. The pathway-specific synapse formation may depend on coordinated activation of LA and ACx neurons, via intercellular anterograde and retrograde

signaling[43]. Furthermore, the remodeling was detectable within hours and continued over days after learning, and it correlated with freezing responses at both 2 h and 3 d, suggesting that the same pathway is involved in both short-term and long-term memory. These results also support the notion that memory consolidation involves gradual structural reorganization outlasting the learning process[44] and that long-term memory becomes increasingly dependent on the cortex with time[45,46].

Fear-memory-related synapse formation specifically at LA–ACx connections could enhance L5 neuronal excitation in ACx by increasing coincident inputs, leading to potential modulation of behaviorally relevant sensory processing. This direct LA–ACx modulation may add to the known indirect cortical modulation by amygdala through its subcortical projections[5,47,48] and may work in concert with cholinergic inputs to L1 during fear memory formation[2]. Although MG–ACx and ACC–ACx connections were not modified by fear learning, they may be involved in other auditory behaviors.

We found that new synapses were formed in an additive manner, by either adding a new spine to an existing bouton or a new bouton to an existing spine. Previous electron microscopy studies have shown preferential contact of new spines on existing boutons[11,49]. Our studies further revealed that new bouton formation on existing spines represents a more frequent event in this additive form of synapse formation. As compared to *de novo* formation of synapses, this additive synapse formation is less demanding for cellular energy, synaptic resources and synaptic space, and thus more suited for circuit remodeling in the adult brain[50]. Finally, although we have observed only a few examples of a new spine replacing an old one on the existing bouton, the possibility remains that new synaptic elements could also compete out existing ones from other pathways.

METHODS

Methods, including statements of data availability and any associated accession codes and references, are available in the online version of the paper.

Note: Any Supplementary Information and Source Data files are available in the online version of the paper.

ACKNOWLEDGMENTS

We thank N. Xu for help with chronic window surgery, Q. Hu for confocal imaging, Y. Kong and B. Zhang for electron microscopy, L. Han for behavioral analysis, L. Zhou for slice recording, and Y. Dan for critical comments and suggestions. This work was supported by grants from Ministry of Science and Technology (973 Program, 2011CBA00400, M.-m.P.) and Chinese Academy of Sciences (Strategic Priority Research Program, XDB02020001, M.-m.P.), and a SIBS-SA scholarship to Y.Y.

AUTHOR CONTRIBUTIONS

Y.Y., D.L. and M.P. designed the experiments. Y.Y. and D.L. performed the experiments and analyzed the data. W.H. performed *in utero* electroporation experiments. Y.S. and J.D. performed the electrophysiology experiments. Y.Z. guided spine data analysis. Y.Y., D.L. Y.Z. and M.P. wrote the paper.

COMPETING FINANCIAL INTERESTS

The authors declare no competing financial interests.

1. Goosens, K.A. & Maren, S. Contextual and auditory fear conditioning are mediated by the lateral, basal, and central amygdaloid nuclei in rats. *Learn. Mem.* **8**, 148–155 (2001).
2. Letzkus, J.J. *et al.* A disinhibitory microcircuit for associative fear learning in the auditory cortex. *Nature* **480**, 331–335 (2011).
3. Peter, M. *et al.* Induction of immediate early genes in the mouse auditory cortex after auditory cued fear conditioning to complex sounds. *Genes Brain Behav.* **11**, 314–324 (2012).
4. Boatman, J.A. & Kim, J.J. A thalamo-cortico-amygdala pathway mediates auditory fear conditioning in the intact brain. *Eur. J. Neurosci.* **24**, 894–900 (2006).
5. Weinberger, N.M. Specific long-term memory traces in primary auditory cortex. *Nat. Rev. Neurosci.* **5**, 279–290 (2004).
6. Moczulska, K.E. *et al.* Dynamics of dendritic spines in the mouse auditory cortex during memory formation and memory recall. *Proc. Natl. Acad. Sci. USA* **110**, 18315–18320 (2013).
7. Denk, W. & Svoboda, K. Photon upmanship: why multiphoton imaging is more than a gimmick. *Neuron* **18**, 351–357 (1997).
8. Harris, K.M. & Kater, S.B. Dendritic spines: cellular specializations imparting both stability and flexibility to synaptic function. *Annu. Rev. Neurosci.* **17**, 341–371 (1994).
9. Grillo, F.W. *et al.* Increased axonal bouton dynamics in the aging mouse cortex. *Proc. Natl. Acad. Sci. USA* **110**, E1514–E1523 (2013).
10. Holtmaat, A., Wilbrecht, L., Knott, G.W., Welker, E. & Svoboda, K. Experience-dependent and cell-type-specific spine growth in the neocortex. *Nature* **441**, 979–983 (2006).
11. Knott, G.W., Holtmaat, A., Wilbrecht, L., Welker, E. & Svoboda, K. Spine growth precedes synapse formation in the adult neocortex in vivo. *Nat. Neurosci.* **9**, 1117–1124 (2006).
12. Lai, C.S., Franke, T.F. & Gan, W.B. Opposite effects of fear conditioning and extinction on dendritic spine remodelling. *Nature* **483**, 87–91 (2012).
13. Xu, T. *et al.* Rapid formation and selective stabilization of synapses for enduring motor memories. *Nature* **462**, 915–919 (2009).
14. Hofer, S.B., Mrsic-Flogel, T.D., Bonhoeffer, T. & Hübener, M. Experience leaves a lasting structural trace in cortical circuits. *Nature* **457**, 313–317 (2009).
15. Zuo, Y., Yang, G., Kwon, E. & Gan, W.B. Long-term sensory deprivation prevents dendritic spine loss in primary somatosensory cortex. *Nature* **436**, 261–265 (2005).
16. Becker, N., Wierenga, C.J., Fonseca, R., Bonhoeffer, T. & Nägerl, U.V. LTD induction causes morphological changes of presynaptic boutons and reduces their contacts with spines. *Neuron* **60**, 590–597 (2008).
17. Romanski, L.M. & LeDoux, J.E. Equipotentiality of thalamo-amygdala and thalamo-cortico-amygdala circuits in auditory fear conditioning. *J. Neurosci.* **12**, 4501–4509 (1992).
18. Malenka, R.C. & Bear, M.F. LTP and LTD: an embarrassment of riches. *Neuron* **44**, 5–21 (2004).
19. Cauller, L. Layer I of primary sensory neocortex: where top-down converges upon bottom-up. *Behav. Brain Res.* **71**, 163–170 (1995).
20. Zhang, S. *et al.* Selective attention. Long-range and local circuits for top-down modulation of visual cortex processing. *Science* **345**, 660–665 (2014).
21. Weinberger, N.M. Physiological memory in primary auditory cortex: characteristics and mechanisms. *Neurobiol. Learn. Mem.* **70**, 226–251 (1998).
22. LeDoux, J.E. Emotion circuits in the brain. *Annu. Rev. Neurosci.* **23**, 155–184 (2000).
23. Armbruster, B.N., Li, X., Pausch, M.H., Herlitze, S. & Roth, B.L. Evolving the lock to fit the key to create a family of G protein-coupled receptors potently activated by an inert ligand. *Proc. Natl. Acad. Sci. USA* **104**, 5163–5168 (2007).
24. Stachniak, T.J., Ghosh, A. & Sternson, S.M. Chemogenetic synaptic silencing of neural circuits localizes a hypothalamus→midbrain pathway for feeding behavior. *Neuron* **82**, 797–808 (2014).
25. Zhu, Y., Wienecke, C.F., Nachtrab, G. & Chen, X. A thalamic input to the nucleus accumbens mediates opiate dependence. *Nature* **530**, 219–222 (2016).
26. De Paola, V. *et al.* Cell type-specific structural plasticity of axonal branches and boutons in the adult neocortex. *Neuron* **49**, 861–875 (2006).
27. Rubio-Garrido, P., Pérez-de-Manzo, F., Porrero, C., Galazo, M.J. & Clascá, F. Thalamic input to distal apical dendrites in neocortical layer 1 is massive and highly convergent. *Cereb. Cortex* **19**, 2380–2395 (2009).
28. Schneider, D.M., Nelson, A. & Mooney, R. A synaptic and circuit basis for corollary discharge in the auditory cortex. *Nature* **513**, 189–194 (2014).
29. Gilmartin, M.R., Balderston, N.L. & Helmstetter, F.J. Prefrontal cortical regulation of fear learning. *Trends Neurosci.* **37**, 455–464 (2014).
30. Senn, V. *et al.* Long-range connectivity defines behavioral specificity of amygdala neurons. *Neuron* **81**, 428–437 (2014).
31. Xiong, Q., Znamenskiy, P. & Zador, A.M. Selective corticostriatal plasticity during acquisition of an auditory discrimination task. *Nature* **521**, 348–351 (2015).
32. Harris, K.D. & Mrsic-Flogel, T.D. Cortical connectivity and sensory coding. *Nature* **503**, 51–58 (2013).
33. Douglas, R.J. & Martin, K.A. Neuronal circuits of the neocortex. *Annu. Rev. Neurosci.* **27**, 419–451 (2004).
34. Feng, G. *et al.* Imaging neuronal subsets in transgenic mice expressing multiple spectral variants of GFP. *Neuron* **28**, 41–51 (2000).
35. Cichon, J. & Gan, W.B. Branch-specific dendritic Ca^{2+} spikes cause persistent synaptic plasticity. *Nature* **520**, 180–185 (2015).
36. Stuart, G.J. & Spruston, N. Dendritic integration: 60 years of progress. *Nat. Neurosci.* **18**, 1713–1721 (2015).
37. Otazu, G.H., Chae, H., Davis, M.B. & Albeanu, D.F. Cortical feedback decorrelates olfactory bulb output in awake mice. *Neuron* **86**, 1461–1477 (2015).
38. Wilson, R.I. & Nicoll, R.A. Endogenous cannabinoids mediate retrograde signalling at hippocampal synapses. *Nature* **410**, 588–592 (2001).
39. Schafe, G.E., Nader, K., Blair, H.T. & LeDoux, J.E. Memory consolidation of Pavlovian fear conditioning: a cellular and molecular perspective. *Trends Neurosci.* **24**, 540–546 (2001).
40. Toni, N., Buchs, P.A., Nikonenko, I., Bron, C.R. & Muller, D. LTP promotes formation of multiple spine synapses between a single axon terminal and a dendrite. *Nature* **402**, 421–425 (1999).

41. Kleindienst, T., Winnubst, J., Roth-Alpermann, C., Bonhoeffer, T. & Lohmann, C. Activity-dependent clustering of functional synaptic inputs on developing hippocampal dendrites. *Neuron* **72**, 1012–1024 (2011).
42. Fu, M., Yu, X., Lu, J. & Zuo, Y. Repetitive motor learning induces coordinated formation of clustered dendritic spines *in vivo*. *Nature* **483**, 92–95 (2012).
43. Park, H. & Poo, M.M. Neurotrophin regulation of neural circuit development and function. *Nat. Rev. Neurosci.* **14**, 7–23 (2013).
44. Caroni, P., Donato, F. & Muller, D. Structural plasticity upon learning: regulation and functions. *Nat. Rev. Neurosci.* **13**, 478–490 (2012).
45. Wiltgen, B.J., Brown, R.A., Talton, L.E. & Silva, A.J. New circuits for old memories: the role of the neocortex in consolidation. *Neuron* **44**, 101–108 (2004).
46. Frankland, P.W. & Bontempi, B. The organization of recent and remote memories. *Nat. Rev. Neurosci.* **6**, 119–130 (2005).
47. Krettek, J.E. & Price, J.L. Amygdaloid projections to subcortical structures within the basal forebrain and brainstem in the rat and cat. *J. Comp. Neurol.* **178**, 225–254 (1978).
48. Gray, T.S., Carney, M.E. & Magnuson, D.J. Direct projections from the central amygdaloid nucleus to the hypothalamic paraventricular nucleus: possible role in stress-induced adrenocorticotropin release. *Neuroendocrinology* **50**, 433–446 (1989).
49. Kirov, S.A., Sorra, K.E. & Harris, K.M. Slices have more synapses than perfusion-fixed hippocampus from both young and mature rats. *J. Neurosci.* **19**, 2876–2886 (1999).
50. Chklovskii, D.B., Mel, B.W. & Svoboda, K. Cortical rewiring and information storage. *Nature* **431**, 782–788 (2004).

ONLINE METHODS

Animals. All procedures were approved by the Animal Committee of the Institute of Neuroscience, Chinese Academy of Sciences. Mice were housed and bred in a 12-h light-dark cycle (7 a.m.–7 p.m. light) in the animal facility of the Institute of Neuroscience. Experiments were performed during the light cycle. C57BL/6 mice were purchased from Slac Laboratory Animals (Chinese Academy of Sciences). YFP-H line mice were obtained from the Jackson Laboratory. Male mice were used for behavioral and imaging experiments. Female mice were used for *in utero* electroporation. Mice used for viral expression were 4 weeks old. Mice used for behavioral experiments and imaging experiments were 7–10 weeks old.

Virus and tracer injection. For virus and Retrobead injection, mice were anesthetized with sodium pentobarbital (7 mg/kg) and positioned in a stereotaxic frame (Reward Co.). Body temperature was maintained at 37 °C using a heating pad. Viruses and Retrobeads (Lumafluor) were injected using a glass micropipette with a tip diameter of 15–20 μm, through a small skull opening (<0.5 mm^2), with a microinjector (QSI). Stereotaxic coordinates for LA: 1.0 mm posterior from bregma, 3.25 mm lateral from the midline, and 3.55 mm vertical from the cortical surface; for MG: 3.15 mm posterior from bregma, 1.8 mm lateral from the midline, and 2.9 mm vertical from the cortical surface; for ACC: 1.00 mm anterior from bregma, 0.5 mm lateral from the midline, and 1.5 mm vertical from the cortical surface; for ACx: 2.5 mm from bregma, 4.5 mm lateral from the midline, and 1.2 mm vertical from the cortical surface.

For AAV-SYN-EGFP, we injected 0.1–0.2 μl (~10^{13} virus particles per ml) into LA, 0.2–0.6 μl into MG, or 1 μl into ACC, and waited 4 weeks for maximal expression before using the mice for *in vivo* imaging. For AAV-SYN-HA-hM4D-ires-mCitrine, AAV-CamKIIa-eArch3.0-2A-EYFP and AAV-CamkIIa-ChR2-mCherry, we injected 0.8–1 μl (~5×10^{12} virus particles per ml) into left LA. For Retrobeads, we injected 0.2 μl into the superficial layers ACx (depth from cortical surface: 0.1 mm) and waited 5–7 d to allow the retrograde labeling. For cholera toxin subunit B (CTB) conjugated to Alexa 488, we applied 0.5 μl (0.5 mg/ml) directly above the ACx to make sure that the CTB was infused into the superficial layers.

***In utero* electroporation.** Pregnant mice at E15.5 were anesthetized with sodium pentobarbital (7 mg/kg) and the abdomen incised to expose the uterus. The plasmid CAG-tdTomato (3 μg/μl) was injected through the uterine wall into the posterior lateral region of the lateral ventricle of embryonic brains with a glass micropipette. Electrical pulses were then delivered to embryos by gently clasping their heads with forceps-shaped electrodes connected to a square-pulse generator CUY21 (Bex Co., Ltd). For each electroporation, five 30-V pulses of 50 ms were applied at 1-s intervals. After the electroporation, the uterine horns were returned to the abdominal cavity, followed by suturing of the abdominal wall and skin.

Surgery. Young adult mice (P42–49) were anesthetized with isoflurane (induction, 4%; maintenance, 1–2%) and fixed in a stereotaxic frame (Reward Co.). Body temperature was maintained at 37 °C using a heating pad. Lidocaine was administered subcutaneously. The muscle covering the auditory cortex was carefully removed with a scalpel. A 2×2 mm^2 region of skull over ACx was removed, exposing the dura. A custom-made double-layered cover glass was used to cover the cortex. UV-cure glue and dental acrylic were used to seal the cover glass. A custom-made stainless steel headplate with a screw hole was embedded into the dental acrylic for repeated imaging. Mice were injected with carprofin (0.3 mg, i.p.) after surgery and were given 2 weeks for recovery before imaging.

For mice used for drug infusion, guide cannulae (26 gauge, with screw caps, Plastics One) were implanted bilaterally with the following coordinates: for ACx: 2.5 mm from bregma, 4.5 mm lateral from the midline, and 1.2 mm vertical from the cortical surface. Implants were affixed to the skull using dental acrylic (Reward Co.). Mice were given 3 d for recovery. For mice used for drug infusion and two photon imaging simultaneously, chronic windows were first implanted in the same way as described above and then guide cannulae were implanted bilaterally into ACx at an angle of 30° to the cortical surface. Animals were returned to their home cage for recovery. Two-photon imaging began 14 d after the surgery.

For mice used for optogenetic manipulation, chronic windows were implanted over ACx, and then ultra-thin green LEDs (APG-1608ZGC/G, Kingbright, 525 nm, 20 mA) were mounted to the chronic windows and cemented onto the skull using dental cement. Mice were given 3 d for recovery before behavioral training.

Local drug infusion. Thirty minutes before fear conditioning or 5 min after fear conditioning, mice were anesthetized with isoflurane, 30-gauge stainless steel injectors attached to 10 μl syringes (Hamilton) were inserted into the guide cannulae, and 0.2 μl of muscimol (0.5 mg/ml) or APV (0.5 μg, 1 μg, 2 μg, 10 μg) per hemisphere was delivered bilaterally at 0.5 μl/min using a two-channel microinfusion pump (Reward Co.). For experiments in **Figures 1f** and **4d**, 1 μl of muscimol was injected into ACx. The spread of drugs was determined by injecting 1 μl of fluorescent solution (FITC, Life Sciences, 5 mM).

In experiments testing the involvement of LA–ACx pathway using the DRREAD system, the right side of ACx was always blocked using muscimol (1 μl at 0.5 μg/μl) in both control and experimental conditions. At 30 min before fear conditioning or recall test, 1 μl clozapine-*N*-oxide (CNO, Sigma, 1 μg/μl) or saline was infused into the left ACx of mice expressing hM4D or EGFP in left LA neurons, at 0.5 μl/min using a two-channel microinfusion pump (Reward Co.).

Brain slice electrophysiology. Mice were anesthetized with isoflurane (Lunan Pharmaceutical) and perfused transcardially with an ice-cold cutting solution containing (in mM) sucrose 213, KCl 2.5, NaH_2PO_4 1.25, $MgSO_4$ 10, $CaCl_2$ 0.5, $NaHCO_3$ 26, and glucose 11 (300–305 mOsm). The brain was rapidly dissected, and coronal 300 μM slices containing the auditory cortex were prepared in the ice-cold cutting solution using a vibratome (Leica VT1200S, Wetzlar, Germany) at slicing speeds of 0.12 mm/s and a blade vibration amplitude of 1 mm. Slices were transferred to the holding chamber and incubated in 34 °C artificial cerebral spinal fluid containing (in mM) NaCl 126, KCl 2.5, NaH_2PO_4 1.25, $MgCl_2$ 2, $CaCl_2$ 2, $NaHCO_3$ 26, and glucose 10 (300–305 mOsm) to recover for 30 min. The slices were then kept at room temperature before recordings. Both cutting solution and ACSF were continuously bubbled with 95%O_2/5%CO_2. Slices were placed on glass coverslips coated with poly-L-lysine (Sigma, St. Louis, MO) and submerged in a recording chamber (Warner Instruments, Hamden, CT). All experiments were performed at near-physiological temperatures (32–34 °C) using an in-line heater (Warner Instruments, Hamden, CT) while perfusing the recording chamber with solution at 3–4 ml/min using a pump (BT100-2J, LongerPump). Whole-cell patch-clamp recordings were made from target neurons under IR-DIC visualization and a CCD camera (IR-1000E, DAGE-MTI) using an Olympus BX51WI microscope (Olympus Optical, Tokyo, Japan). Patch pipettes were filled with a Cs^+-based, low-Cl^- internal solution containing (in mM) $CsMeSO_3$ 130, $MgCl_2$ 1, $CaCl_2$ 1, HEPES 10, QX-314 2, EGTA 11, Mg-ATP 2, Na-GTP 0.3 (pH 7.3, 295 mOsm).

To assess the effects of local CNO infusion in ACx on synaptic transmission of LA axons, we first co-injected AAV-hM4D and AAV-ChR2 into LA. Brain slices were prepared 3 weeks after virus expression. L5 pyramidal neurons in ACx were recorded using whole-cell patch clamp. To record light-evoked EPSCs, 5-ms, 5-mW blue light (laser: UHP-Mic-LED-475, Prizmatix, Israel) was delivered through the objective to the superficial layers of ACx. Light-evoked EPSCs were recorded before and after perfusion with CNO (6 μM).

Behavior. Fear conditioning and behavioral test for freezing responses took place in different environments. Mice were handled and habituated before conditioning. A custom-made cage ($22 \times 28 \times 40$ cm) with an electrifiable floor connected to a shock generator (MED) was used for conditioning, and a new context—a round cage (diameter 20 cm, height 40 cm) with a plastic floor—was used for behavioral test. Both cages were soundproofed. Before conditioning, the conditioning cage was wiped clean with 70% ethanol. Before behavioral testing, the test cage was wiped clean with water and sprayed with scented water. The behavior was captured with a camera and recorded with a surveillance system. A custom-made software written using Presentation (Neurobehavioral Systems) was used to control the delivery of sound and foot shocks. The conditioned stimulus was a series of 0.5-s, 14-kHz tone beeps interleaved with 0.5 s silence, lasting 10 s, at 80 dB, and the unconditioned stimulus was a 2-s, 0.5-mA foot shock. For mice in behavioral experiments, each mouse was exposed to one presentation of sound and foot shocks. For conditioned mice in imaging experiments, each mouse received five repeats of 10 s sound that co-terminated with the 2-s foot shock. For controls in imaging experiments, five repeats of sound and foot shocks were presented pseudorandomly without overlapping. The behavioral responses to CS were tested once, 1 d after conditioning, for both conditioned and control animals, using a CS sound lasting 60 s. Freezing behavior was scored using Noldus (Noldus Information Technology). The mice were considered to be freezing when

doi:10.1038/nn.4370

no obvious difference (non-overlapping region below 10% of the body size) was detected in the images from the video for 2 s. The automatic scoring was verified by an experimenter blind to the experimental conditions. The video recorded 60 s before the test was scored as a basal level of freezing, which was subtracted from the freezing time during the test. For chemogenetic (hM4D) and optogenetic (eArch3.0) silencing experiments, we silenced the right side of ACx with muscimol and inhibited LA–ACx pathway on the left side only, owing to the low success rate in targeting LA for virus injections.

Two-photon microscopy. Mice were anesthetized with isoflurane (induction, 4%; maintenance, 1%) and fixed using the implanted headplate. Image stacks were taken every 0.7 μm, from the cortical surface to 100–150 μm deep, with a two-photon microscope (Sutter) controlled by Scanimage (Janelia). The objective used was 25×, 1.05 numerical aperture (Olympus). A digital zoom of 6 was used. A Ti:sapphire laser (Spectra Physics) was used as the light source and tuned to 920 nm for imaging. YFP and GFP signals were obtained using filters 495/40 and 535/50 (Chroma). The 535/50 filter (channel 1) collected both GFP and YFP signals; the 495/40 filter (channel 2) collected GFP-only signals. By subtracting GFP signals from channel 1 signals, we obtained YFP-only images. Mice were first imaged 1 d before conditioning. The second imaging session took place 2 h after conditioning. Some mice (data in **Fig. 6c**) were imaged daily and others were imaged again 3 d after conditioning.

Data analysis. All images were analyzed using ImageJ, blind to experimental conditions. For bouton identification, we adopted criteria from ref. 22. The fluorescence intensity was profiled along identified axons using ImageJ. Bright swellings were identified as boutons when the peak intensity was over three times brighter than the axon shaft. Spine identification criteria were the same as described in ref. 11. For the dual-color images, a potential bouton–spine pair was visually identified as described in ref. 13, when a presynaptic bouton and a postsynaptic spine overlaid in the image plane.

For formation and elimination assays of boutons, spines, or bouton–spine pairs, reconstructed 3D images were used to minimize imaging distortion caused by movements and rotation between imaging intervals. Formation and elimination of bouton (or spine, or bouton–spine pairs) were based on comparison of the images collected at two different time points (2 h vs. 1 d before conditioning, or 3 d vs. 1 d before conditioning, in **Figs. 1** and **2**). Percentages of stable, eliminated and newly formed boutons (or spines, or bouton–spine pairs) were all normalized to the initial image at −1 d. The total number of boutons (or spines) analyzed for each individual mouse was >200, and that of synaptic pairs was around 100. Data are presented as mean ± s.e.m. across animals. Correlation between two parameters was modeled using linear regression and fitted using Matlab curve fitting toolbox.

Statistics. No statistical methods were used to predetermine sample sizes, but our sample sizes are similar to those generally employed in the field. No data point was excluded. Two-sided unpaired Student's *t*-tests were used for freezing behavior comparisons between different groups. Two-sided paired Student's *t*-tests were used for paired comparisons in **Figures 1f** and **5** and **Supplementary Figure 10**. Data distribution of mouse freezing responses and spine or bouton turnover rates was assumed to be normal, but this was not formally tested. Mann-Whitney *U*-test was used for comparisons in imaging data. Kolmogorov–Smirnov test was used for **Figure 6c**. *F* test was used for test the significance for linear regression in **Supplementary Figure 7**. Statistical test used, test statistics and the *P* values are shown in figure legends. The relevant test statistics—for example, *t*-values and degrees of freedom for *t*-tests or *U*-values for Mann-Whitney *U*-test—are also shown in figure legends. A **Supplementary Methods Checklist** which includes a summary of statistics is available.

Histology. After completion of imaging or tracing, mice were deeply anesthetized and transcardially perfused with 0.1 M phosphate-buffered saline (PBS) solution, which was followed with 4% paraformaldehyde (PFA) in PBS. Brains were postfixed in the same PFA solution overnight and dehydrated using 30% sucrose. Coronal brain sections of 20–50 μm were cut using a vibratome (Leica Microsystems) and imaged on a stereoscope (Nikon E80i) or confocal microscope (Nikon A1R) to check virus expression.

Electron microscopy. Mice were deeply anesthetized and transcardially perfused with PBS and then with 4% PFA and 0.5% glutaraldehyde in 0.1 M PBS. The ACx was dissected out with scalpel blade and was immersed in the same fixation solution for 4–6 h at 4 °C, then dehydrated in ascending ethanol series, and finally embedded in araldite for 2 d. Ultrathin slices (70 nm) were cut from the superficial regions of ACx (10–100 μm from the pial surface) to target L1 of ACx, where the *in vivo* images were obtained, and then collected on nickel grids (200 mesh). For immunogold electron microscopy, YFP-H mice injected with AAV-Cre virus in LA were used. Nonspecific binding was blocked by 1% BSA. Slices were incubated at 4 °C for 48 h with primary antibodies: 1:40 mouse anti-GFP (Sigma, SAB2702197) for staining apical dendrites that expressed YFP and 1:40 rabbit anti-Cre (Sigma, SAB2700194) for staining LA axons infected with AAV-Cre. After washed five times for 15 min each with 0.1 M PBS, slices were incubated with anti-mouse (15 nm, 1:100, Ted Pella, 15752) and anti-rabbit (5 nm, 1:100, Ted Pella, 15725) gold conjugates for 2 h at room temperature. Slices were then washed with five times for 15 min each in 0.1 M PBS and incubated with 1% glutaraldehyde to fix the Nanogold particles. Ultra-thin sections were incubated with methanolic uranyl acetate and lead citrate before observed with a Joel JEM-1230 TEM at the electron microscopy core facility in ION.

Data availability. The data that support the findings of this study are available from the corresponding author upon request.